In THF the negative charge was delocalized to a larger extent on the living chain end of 1PB[12] and 2PB[13] than on that of St and Bd. The low block efficiencies observed in THF medium may be the result of the delocalization of charge on the chain end. Furthermore, comparing 1PB with 2PB, 2PB has a more delocalized living chain end and consequently may have a lower block efficiency than 1PB. On the other hand, in toluene for all cases studied the block efficiencies are high and almost 100%. We cannot explain this drastic change with changes in negative charge delocalization, since we have concluded by means of NMR spectroscopy that the living chain ends of 1PB and 2PB have similar charge distributions in THF and hydrocarbon media. In THF a solvent-separated ion pair is predominant, whereas in toluene the chain end is visualized as a contact ion pair. Such different types of ion pairs may be responsible for the drastic change in the block efficiency observed in this study.

References and Notes

(1) Suzuki, T.; Tsuji, Y.; Takegami, Y. *Macromolecules* **1978**, *11*, 639.
(2) Suzuki, T.; Tsuji, Y.; Takegami, Y.; Harwood, H. J. *Macromolecules* **1979**, *12*, 234.
(3) Morton, M.; Ells, F. R. *J. Polym. Sci.* **1962**, *61*, 25.
(4) O'Driscoll, K. F.; Kuntz, I. *J. Polym. Sci.* **1962**, *61*, 19.
(5) Narita, T.; Masaki, A.; Tsuruta, T. *J. Macromol. Sci., Chem.* **1970**, *A4*, 277.
(6) Narita, T.; Tsuruta, T. *J. Organomet. Chem.* **1971**, *30*, 289.
(7) THF and toluene[8] can serve as transfer agents in the anionic polymerization systems. Our results show no influence of these transfer steps. After the reaction time all the BuLi's are reacted completely in toluene as well as in THF.
(8) Gatzke, A. L. *J. Polym. Sci., Part A-1* **1969**, *7*, 2281.
(9) The chromatograph and its four μ-Styragel columns provide insufficient resolution for high molecular weight samples. Therefore, we carried out the block copolymerizations for a low molecular weight range.
(10) The molar absorptivity for each homopolymer, which depends on the microstructure, decreases as follows: poly-2PB > poly-1PB > poly-St.
(11) Shima, M.; Bhattacharyya, D. N.; Smid, J.; Szwarc, M. *J. Am. Chem. Soc.* **1963**, *85*, 1306.
(12) Suzuki, T.; Tsuji, Y.; Watanabe, Y.; Takegami, Y. *Polym. J.* **1979**, *11*, 651.
(13) Suzuki, T.; Tsuji, Y.; Watanabe, Y.; Takegami, Y. *Polym. J.* **1979**, *11*, 937.

Domain-Boundary Structure of Styrene–Isoprene Block Copolymer Films Cast from Solutions. 6. Effect of Temperature on Spherical Microdomain Structure

Mineo Fujimura,† Hiroshi Hashimoto,‡ Koichiro Kurahashi,§ Takeji Hashimoto,* and Hiromichi Kawai

Department of Polymer Chemistry, Faculty of Engineering, Kyoto University, Kyoto 606, Japan.

Received November 6, 1980

ABSTRACT: The effect of heating on the spherical microdomain structure was investigated for a particular diblock polymer of polystyrene and polyisoprene. The radius of the sphere and interdomain distance are observed to increase slightly with increasing temperature from room temperature to 180 °C. The observation is interpreted as follows. The original domain structure is in a nonequilibrium state in that the number of block polymer molecules per domain in the real system (and therefore the size of the spherical domain and interdomain distance) is far less than that in the equilibrium state. As the system is heated, it tends to approach equilibrium, resulting in an increased number of block polymer molecules per domain and therefore in increased interdomain distance and size of the domain. The thickness of the interfacial region in which the unlike segments intermix tends to increase with increasing temperature by an amount which can be predicted from the temperature dependence of the Flory–Huggins interaction parameter χ.

I. Introduction

It is well-known that the repulsive interaction between polystyrene and polyisoprene block sequences in the block polymer causes microphase separation, resulting in a microdomain structure with a size determined primarily by the molecular dimensions of the respective sequences.[1-8] The low compressibility of polymeric solid demands uniform filling of the domain space by the respective segments,[4,5] which further specifies the most stable shape of the domain; e.g., a spherical microdomain is most stable when the molecular volume of one of the block sequences is very large compared with the others.

In a previous paper[6] in this series we clarified equilibrium and nonequilibrium aspects of the spherical domains observed in solvent-cast films. The spherical domain is not in a state of equilibrium in that the number of block polymer molecules per domain, N, in real systems is far less than the value in the equilibrium state, resulting in the size of the domain (e.g., the radius of the A domain) and interdomain distance D being much less than the equilibrium values:

$$(4\pi/3)R_A^3 = N\bar{v}_A \quad (1)$$

$$\epsilon D^3 = N(\bar{v}_A + \bar{v}_B) \quad (2)$$

where $\bar{v}_K$ is the molecular volume of the K-block chain[19] and ϵ is the packing constant of the spherical domains (ϵ being $1/\sqrt{2}$ in the case of hexagonal close packing). However, conformations of the respective chain molecules within the domain space are close to those in the equilibrium state, giving rise to a $^2/_3$ power law[6,7] in the mo-

† Present address: Research and Development, Japan Synthetic Rubber Co., Ltd., Tama-ku, Kawasaki 214, Japan.
‡ Present address: Research Laboratories, Fujinomiya, Fuji Photo Film, Co., Ltd., Fujinomiya City, Shizuoka 418, Japan.
§ Present address: Research and Development, Sumitomo Rubber Industry, Ltd., Tsutsui-cho, Fukiai-ku, Kobe 651, Japan.

0024-9297/81/2214-1196$01.25/0

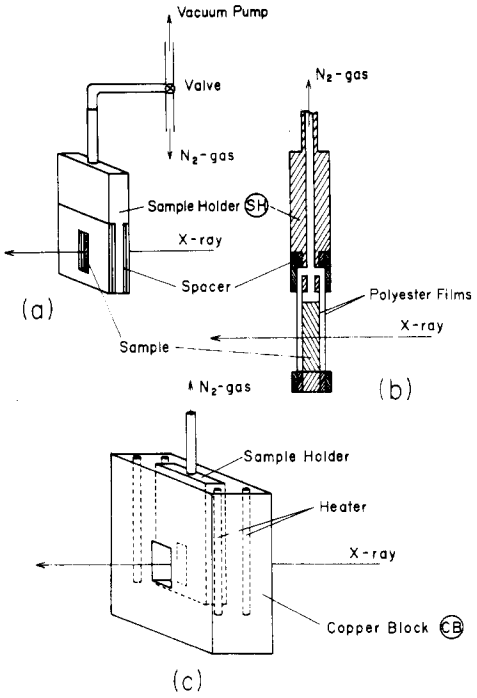

Figure 1. Schematic diagram of the temperature cell used in this experiment: CB, a copper block with heating elements and temperature controller; SH, a specimen holder sealed with N_2 gas to reduce oxidation.

lecular weight dependence of R_A and D; i.e., $R_A \sim M_A^{2/3}$ and $D \sim (M_A + M_B)^{2/3}$, where M_K is the molecular weight of the K-block chain.

The nonequilibrium aspect of the spherical microdomain is encountered in the solvent evaporation process.[6,7] During the solvent evaporation, the system attains a new equilibrium by changing N. N tends to increase with increasing concentration. In the lamellar or cylindrical domains N can be increased simply by a shrinking along the interface, i.e., by a decrease of the distance between adjacent chemical junction points along the interface. However, the spherical domain can change its size only by a process involving transport of A (B) chains through the matrix of B (A) chains. This process must overcome a larger energetic barrier than that involved in the lamellar or cylindrical domains. This is the main reason that the nonequilibrium effect of the spherical domain is large compared with that of the lamellar domain as reported in previous works.[6,8] The energetic barrier increases with increasing concentration to result in N being fixed at a certain concentration. The solvent is further removed but the system cannot attain a new equilibrium; i.e., N does not increase. R_A and D change only through changes of $\bar{v}_A$ and $\bar{v}_B$ above this concentration, giving rise to decreasing R_A and D with increasing concentration.

In this paper we investigate the effect of heating the spherical microdomain on the average values of R_A, D, the distributions of R_A and D, and the characteristic interfacial thickness, ΔR, to study further the equilibrium and nonequilibrium aspects of the spherical microdomain.[18]

II. Experimental Section

A particular styrene–isoprene diblock polymer, SI-10 (designated as SI-4 in previous paper[6]), is used for the present studies. The block polymer has a total number-average molecular weight of 2.2×10^5 and a polyisoprene content of 15.4 wt %. Film specimens were prepared by casting a 10 wt % toluene solution, containing a small amount of N-phenyl-β-naphthylamine (1 wt % of the block polymer) to reduce the effect of oxidative degradation upon heating, onto a glass plate. The solvent-cast films were dried under a vacuum of 10^{-6} torr for several days until the specimens were at constant weight.

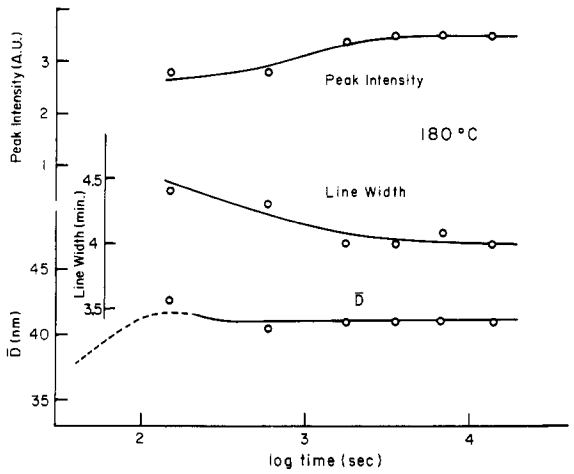

Figure 2. Changes of the interdomain distance $\bar{D}$, peak intensity, and line width of the first-order scattering maximum with time after the specimen is heated to 180 °C.

A detailed characterization (microstructure of polyisoprene, microdomain structure, statistical segment lengths, etc.) of the block polymer is given elsewhere.[6,9]

Figure 1 schematically represents the temperature cell used in this experiment. The cell is essentially composed of two parts: a copper block (CB) with heating elements and a temperature controller, and a specimen holder (SH) (Figure 1a,b) in which a film specimen or molten specimen is enclosed. As shown in parts a and b of Figure 1, two windows (for the incident and scattered X-rays) are doubly sealed by thin mylar films (of 6-μm thick). The specimen is inserted into the sample holder (3-mm thick along the X-ray path × 4-mm wide × 20-mm long), which as shown in Figure 1a, is first evacuated and then filled with N_2 gas. The sample holder is then inserted in the metal block at the measuring temperature, as shown in Figure 1c. The metal block is mounted on an xy stage so as to adjust its center to the incident X-ray beam.

The extent of oxidative degradation under these measuring conditions at 180 °C was investigated by inserting styrene–butadiene–styrene (SBS) triblock polymers (having block molecular weights of 14 000/30 000/14 000, respectively) in the temperature cell. It turned out that the specimen containing 1 wt % N-phenyl-β-naphthylamine was stable when it was enclosed in cell for at least 6 h at 180 °C.

The microdomain structure was investigated as a function of temperature by small-angle X-ray scattering (SAXS). Two SAXS apparatuses were used for this purpose: (i) a four-slit Beeman's step-scanning SAXS goniometer, with Soller slits inserted between the third and fourth slits, and (ii) a SAXS apparatus with a linear position-sensitive proportional counter (PSD). The detailed optical arrangement of the slits, focal spot, sample, and detector is given elsewhere.[10-12] Both apparatuses utilize rotating-anode X-ray generators (RU-A and Z, Rigaku-Denki), operated at 40 kV and 200 mA for apparatus (i) and 55 kV and 200 mA for apparatus (ii).

The SAXS results were corrected for absorption and background scattering (air scattering plus parasitic scattering) and were desmeared for collimation errors in both the slit-length and slit-width directions.

III. Results

The microdomain structure was first investigated on as-cast films at room temperature. Then it was investigated at 180 °C after the same film specimen was heated at 180 °C for 30 min in the temperature cell as described above. The film specimen was then quenched to room temperature (designated as "quenched specimen") by quickly removing the sample holder (SH) from the heated metal block (CB).

1. Thermal History. In order to measure the time required for the domain structure to achieve a new equi-

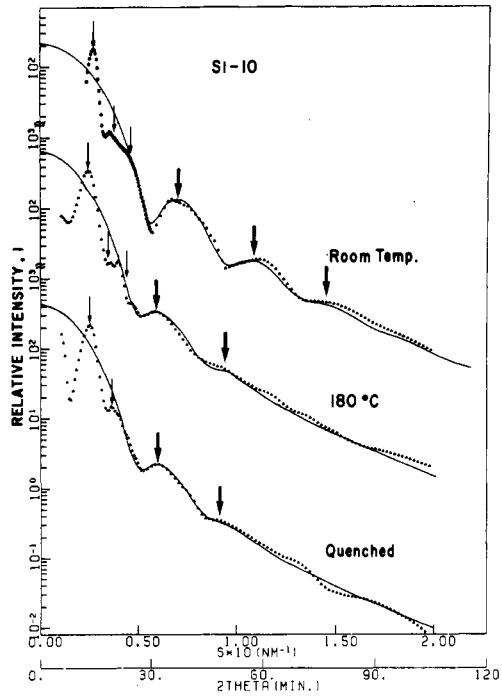

Figure 3. Desmeared SAXS profiles (desmeared for both slit-length and slit-width weighting functions) from the as-cast specimen, the specimen at 180 °C, and the quenched specimen. $s = (2 \sin \theta)/\lambda$.

librium when the temperature of the specimen is raised to 180 °C, we investigated, using the SAXS apparatus with the PSD (measuring time 100 s), the change in the SAXS curves with time after the sample cell (SH) was put into the metal block (CB) controlled at 180 °C. A summary of the results is shown in Figure 2, in which the peak intensity and line width of the first-order scattering maximum and the average nearest-neighbor distance, $\bar{D}$, calculated from the first-order peak by Bragg's equation ($2\bar{D} \sin \theta = \lambda$, 2θ being the scattering angle) are plotted as a function of time after the cell is heated at 180 °C. The temperature of the specimen reaches 180 °C within 1 min after the cell is heated at 180 °C. It is shown that the domain structure seems to reach a new equilibrium state within 30 min, after which the peak intensity, peak breadth, and $\bar{D}$ hardly change.

Thus the small-angle scattering curve at 180 °C as shown in Figure 3 was measured by the SAXS apparatus with the PSD 30 min after the specimen was heated at 180 °C in the temperature cell. The measuring time was 1800 s. The measurement of the SAXS curve at 180 °C in the large-angle region as shown in Figure 4 was also carried out by the SAXS apparatus with the step-scan goniometer 30 min after the specimen was heated to 180 °C in the temperature cell. The measuring time in this case was 21 600 s.

2. Temperature Dependence of Domain Size and Interdomain Distance. The SAXS profiles were measured for the as-cast film at room temperature and at 180 °C and for the quenched sample at room temperature. Figure 3 shows the SAXS profiles corrected for absorption, air scattering, and collimation errors in both the slit-width and slit-height directions. The profiles were also corrected for the background scattering, I_b, arising from thermal diffuse scattering within each phase; i.e., I_b was subtracted from the total desmeared intensity.

All the measured and corrected SAXS profiles (shown by solid triangles) exhibit scattering profiles typical for an assembly of spherical microdomains in a cubiclike macrolattice. Thus the profiles exhibit a number of scattering

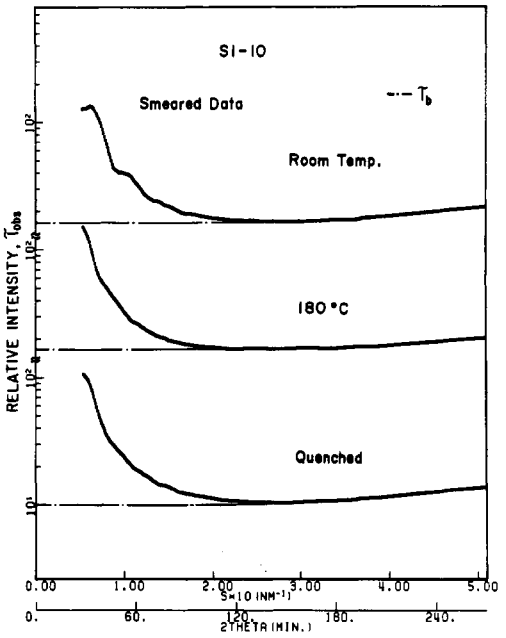

Figure 4. Smeared SAXS profiles $\tilde{I}_{obsd}$ at large-angle tails and estimated background scattering profiles $\tilde{I}_b$ from the as-cast specimen, the specimen at 180 °C, and the quenched specimen.

maxima or shoulders which originate either from interparticle interference (the peaks and shoulders marked by thin arrows) or from intraparticle interference (the broad peaks marked by thick arrows).

The scattering maxima due to interparticle interference appear at the scattering angle $2\theta_{m1}$, corresponding to the average nearest-neighbor distance $\bar{D}$ between the polyisoprene spheres, and at scattering angles of $\bar{D}/\sqrt{2}$ and $\bar{D}/\sqrt{3}$ of the scattering of the first-order maximum:

$$2\bar{D} \sin \theta_{m1} = \lambda \tag{3}$$

where λ is wavelength of the X-rays and $2\theta_{m1}$ is the scattering angle of the first-order maximum. The full width at half-maximum (fwhm), W_D, was also estimated for the first-order scattering maximum from each specimen.

As the scattering vector $\mathbf{s}$ increases, where

$$|\mathbf{s}| = (2 \sin \theta)/\lambda \tag{4}$$

the interference function approaches unity, and in the large s region, the scattering from an assembly of the spheres can be described by "independent scattering"; i.e., the total intensity is equal to the intensity from an isolated sphere times a number of spheres. The broad scattering maxima marked with the thick arrows are the maxima in the independent scattering from isolated spheres. If the distribution of radii of the spheres is given by $P(R)$, then the independent scattering is given by

$$I(s) = \int_0^\infty dR\, P(R) I(s;R) / \int_0^\infty dR\, P(R) \tag{5}$$

where $I(s;R)$ is the scattered intensity from a single sphere having a radius R.

$I(s;R)$ is given by[6]

$$I(s;R) = (\text{const}) R^6 \Phi^2(u) \exp(-4\pi^2\sigma^2 s^2) \tag{6}$$

where

$$\Phi(u) = 3(\sin u - u \cos u)/u^3 \tag{7}$$

and

$$u = 2\pi R s \tag{8}$$

Table I
Effect of Temperature on Domain Properties of a Particular Spherical Microdomain

condition	spacing $\bar{D}$, nm exptl	spacing $\bar{D}$, nm calcd[a]	$\sigma_d/\bar{D}$	radius $\bar{R}$, nm exptl	radius $\bar{R}$, nm calcd[a]	$\sigma_r/\bar{R}$	N[b] exptl	N[b] calcd[a]	domain boundary ΔR, nm exptl	domain boundary ΔR, nm calcd[a]
room temp	37.3	87.0	0.14	12.7	26.7	0.09	140	1300	2.1	1.4
180 °C	41.0	75.0	0.18	14.4	23.1	0.13	187	770	2.5	2.0
quenched	39.5	87.0	0.17	14.2	26.7	0.13	196	1300	1.8	1.4
		(80.2)			(24.7)			(1030)		(1.7)

[a] Helfand and Wasserman.[7] [b] From eq 1.

σ is a parameter associated with the thickness of the diffuse boundary in the spherical domains, discussed in detail in the next section.

In this analysis we assume a Gaussian function for the size distribution

$$P(R) = (2\pi\sigma_r^2)^{-1/2} \exp[-(R - \bar{R})^2/2\sigma_r^2] \quad (9)$$

where $\bar{R}$ is the average radius of the spheres and σ_r is its standard deviation. The solid lines in Figure 3 show a best fit of the calculated independent scattering and measured scattering curves, the values of $\sigma_r/\bar{R}$ and $\bar{R}$ thus estimated being summarized in Table I.

3. Domain-Boundary Thickness. The domain-boundary thickness in the spherical microdomains is estimated according to the methods described in detail in the previous paper,[6] i.e., according to the methods based on full analyses of either smeared or desmeared data in the large-angle tails of the SAXS curves.

Figure 4 shows the smeared SAXS curves at the large-angle tails, where the SAXS intensities tend to increase with increasing s due to the increasing contribution from the thermal diffuse scattering within each domain. This background scattering, $\tilde{I}_b$, was subtracted from the total scattering, $\tilde{I}_{obsd}$, for further analysis on domain-boundary thickness. $\tilde{I}_b$ was estimated according to an empirical procedure proposed by Vonk[13]

$$\tilde{I}_b = as^n + b \quad (10)$$

where the parameters a, b, and n are determined from the least-squares fit of the measured curve over a sufficiently wide angluar range.

Figure 5 shows a plot of ln $(s^3\tilde{I})$ vs. s^2 based on a full analysis of the smeared data, i.e., the analysis which is proposed to be a useful approach in the previous paper.[6] The smeared intensity, $\tilde{I}$, is corrected for the background intensity, $\tilde{I}_b$; i.e., $\tilde{I} = \tilde{I}_{obsd} - \tilde{I}_b$. The analysis involves an estimation of σ associated with the domain-boundary thickness from a nonlinear least-squares curve fitting of the data on $s^3\tilde{I}$ (circles) with the smeared theoretical intensity s^3I_{theor} (solid curve)

$$s^3\tilde{I}_{theor}(s) = (\text{const})\{[1 - 2s^2(p^2 + 4\pi^2\sigma^2)] \times \text{Erfc}\,[s(p^2 + 4\pi^2\sigma^2)^{1/2}] \exp(s^2p^2) + s(p^2 + 4\pi^2\sigma^2)^{1/2} \exp(-4\pi^2\sigma^2s^2)\} \quad (11)$$

where p is a parameter associated with a Gaussian weighting function along the slit height, $W_l(u)$

$$W_l(u) = W_l(0) \exp(-p^2u^2) \quad (12)$$

From the best fits one can estimate σ and then the characteristic interfacial thickness ΔR, defined by

$$\Delta R = \Delta\rho/|d\eta(r)/dr|_{r=R} = \sqrt{2\pi}\,\sigma \quad (13)$$

The function $\eta(r)$ in eq 13 is the electron density variation of the spherical domain in the radial direction r across the interface. $\eta(\mathbf{r})$ is given by a three-dimensional

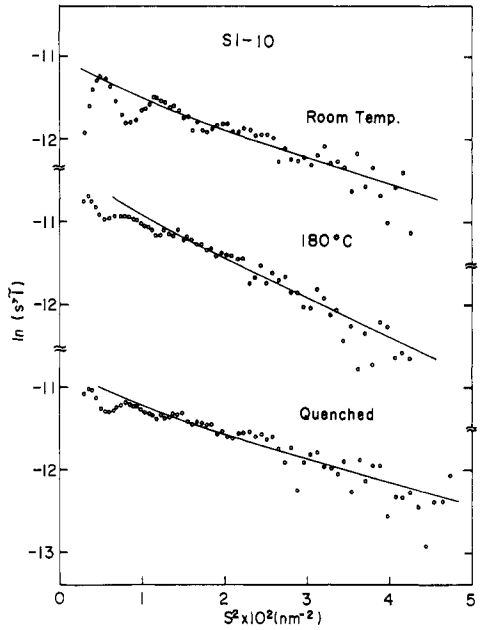

Figure 5. Plots of ln $(s^3\tilde{I})$ vs. s^2 based on a full analysis on the smeared data to estimate σ associated with the domain-boundary thickness. The open circles and the solid curves are the measured data and the results of the best nonlinear curve fitting of the smeared theoretical intensity, $\tilde{I}_{theor}$, respectively. $\tilde{I} = \tilde{I}_{obsd} - \tilde{I}_b$. $s = (2 \sin\theta)/\lambda$.

convolution product of $\rho(\mathbf{r})$ and a Gaussian smoothing function $h(\mathbf{r})$ with a standard deviation σ:

$$\eta(\mathbf{r}) = \rho(\mathbf{r}) * h(\mathbf{r}) \quad (14)$$

$$h(\mathbf{r}) = (2\pi\sigma^2)^{-3/2} \exp(-r^2/2\sigma^2) \quad (15)$$

$\Delta\rho$ is an excess electron density of the spherical domain relative to the matrix. $\rho(\mathbf{r})$ has a constant value of $\Delta\rho$ within the sphere of radius R and is zero outside the sphere. The characteristic interfacial thickness ΔR thus estimated is also summarized in Table I.

IV. Discussion

1. Domain Size and Interdomain Distance. It is shown in Table I that both the interdomain distance $\bar{D}$ and the domain size $\bar{R}$ increase slightly with increasing temperature from room temperature to 180 °C. The values $\bar{D}$ and $\bar{R}$ slightly decrease by quenching the specimens from 180 °C to room temperature.

The experimental observations on the changes of $\bar{D}$ and $\bar{R}$ with temperature are unexpected and surprising in view of the thermodynamics of the microdomain structure. When the temperature is raised, the repulsive interaction between polystyrene and polyisoprene block chains decreases and therefore the Flory-Huggins interaction parameter χ_{SI} between the two block chains decreases, which tends to decrease the constraint-volume effect, i.e., A (B)

chains being restricted to A (B) domains. At elevated temperatures, A (B) chains can take some random walks in the B (A) domains which are prohibited at lower temperatures, resulting in increased mixing and decreased values of $\bar{D}$ and $\bar{R}$. This prediction is opposite to the experimental results.

More quantitatively, we can analyze changes in the values of $\bar{R}$ and $\bar{D}$ in the equilibrium state on the basis of the theory developed by Helfand and Wasserman in the context of the narrow-interphase approximation,[7] as in our previous paper, in which we compared theoretical and experimental values of $\bar{R}$ and $\bar{D}$ as a function of molecular weights of the block polymers.[6]

We now calculate temperature dependences of $\bar{R}$ and $\bar{D}$. We assume that the temperature dependences of the Kuhn statistical segment lengths for polystyrene (b_{PS}) and polyisoprene (b_{PI}) are negligibly small and equal to the values used in the previous paper:[6]

$$b_{PS} = 0.68 \qquad b_{PI} = 0.59 \qquad \text{(nm)} \tag{16}$$

The densities of pure polymers at room temperature are

$$\begin{aligned} (\rho_0)_{PS} &= 1.01 \times 10^4 \\ (\rho_0)_{PI} &= 1.36 \times 10^4 \qquad (\text{mol/m}^3) \end{aligned} \tag{17}$$

and the thermal expansion coefficients are

$$\begin{aligned} \alpha_{PS} &= 2.1 \times 10^{-4} \quad (\text{for } T < T_{g,PS}) \\ &= 6.1 \times 10^{-4} \quad (\text{for } T > T_{g,PS}) \qquad (\text{deg}^{-1}) \end{aligned} \tag{18}$$

$$\alpha_{PI} = 6.7 \times 10^{-4} \qquad (\text{deg}^{-1}) \tag{19}$$

As for the interaction parameter Ω, we adopted a result reported by Rounds and McIntyre as cited by Helfand

$$\Omega = (\delta_{PS} - \delta_{PI})^2/RT \tag{20a}$$

$$= -900 + 7.5 \times 10^5/T \qquad (\text{mol/m}^3) \tag{20b}$$

where δ_A is the solubility parameter of the A-block chain.

The equilibrium values calculated from the theory with the parameters described above are summarized in Table I. The values in parentheses for the quenched samples are calculated by setting the temperature at 100 °C rather than 25 °C, since the equilibrium aspects of the domain morphology may be fixed at the temperature of the polystyrene glass transition. As one would expect the equilibrium values of $\bar{R}$ and $\bar{D}$ tend to decrease slightly with increasing temperature, which is primarily due to decreasing the interaction parameter Ω.

It is very important to note that the experimental $\bar{R}$ and $\bar{D}$ are very much less than the predicted values, as already discussed in detail in the previous paper.[6] This discrepancy in $\bar{R}$ and $\bar{D}$ is attributed to a nonequilibrium effect encountered during the solvent evaporation process. During the solvent evaporation, the system attains a new equilibrium by changing the domain size $\bar{R}$ and interdomain distance $\bar{D}$, which, in turn, involves a change in the number N of block chains per spherical domain (see eq 1 and 2). The spherical domain can change its size only by a process involving a transport of A chains through the matrix of B chains, a process which must overcome an energy barrier attributed to A–B interactions. The energy barrier increases with increasing concentration to result in the domain morphology (i.e., the value N) being fixed at a certain concentration. The solvent is further removed from the system, but N is fixed; i.e., the system cannot achieve equilibrium. $\bar{v}_A$ and $\bar{v}_B$ are the only quantities which vary with solvent evaporation. Therefore the spherical domain system is not in equilibrium in terms of N (giving rise to $\bar{R}$ and $\bar{D}$ smaller than the equilibrium values by the same fraction, as experimentally found), but the chain conformation in a given domain and matrix follows closely that of the equilibrium state. Therefore the increase of experimental $\bar{R}$ and $\bar{D}$ values with increasing temperature can best be interpreted as a consequence of the system tending to approach equilibrium. The transport of A chains (forming the spheres) through the matrix of B chains in bulk must overcome a large energy barrier arising from A–B thermodynamic interaction and hydrodynamic interaction. Therefore the system cannot attain a true equilibrium within the time scale of the experiments, although the system tends to approach equilibrium.

Table II
Changes in $\bar{D}$ and $\bar{R}$ of the Spherical Domain with Temperature

condition	$\bar{D}_{180°C}/\bar{D}_{\text{room temp}}$ exptl[a]	$\bar{D}_{180°C}/\bar{D}_{\text{room temp}}$ calcd[b]	$\bar{R}_{180°C}/\bar{R}_{\text{room temp}}$ exptl[a]	$\bar{R}_{180°C}/\bar{R}_{\text{room temp}}$ calcd[b]
room temp → 180 °C	1.10	1.02	1.13	1.03
180 °C → room temp	1.04	1.02	1.01	1.03

[a] From Table I. [b] Thermal expansion or contraction only.

Decreases in $\bar{R}$ and $\bar{D}$ by quenching the specimen from 180 °C to room temperature can best be interpreted totally as a nonequilibrium effect. That is, if the system follows equilibrium the values should increase primarily due to an increase of the value of N with decreasing temperature. In reality the system does not follow equilibrium within the time scale of the quenching, so the number N is fixed and, consequently, in this sense the domain morphology is fixed. $\bar{R}$ and $\bar{D}$ decrease simply due to the decrease of the molecular volume $\bar{v}_D$ and $\bar{v}_A + \bar{v}_B$, respectively, i.e., due to an increase of mass density.[19,20]

Table II shows changes in $\bar{D}$ and $\bar{R}$ with temperature in the context of nonequilibrium effects, i.e., the temperature effects being brought totally from thermal expansions and contraction with a fixed number N. We define $\bar{D}_{180°C}$ and $\bar{R}_{180°C}$ as the $\bar{D}$ and $\bar{R}$ values at 180 °C and $\bar{D}_{\text{room temp}}$ and $\bar{R}_{\text{room temp}}$ as those at room temperature. Table II summarizes the ratios $\bar{D}_{180°C}/\bar{D}_{\text{room temp}}$ and $\bar{R}_{180°C}/\bar{R}_{\text{room temp}}$ as found experimentally (from Table I) and theoretically during the heating (room temperature → 180 °C) or quenching (180 °C → room temperature). The calculated and measured ratios agree within the experimental errors in the case of the quenching, indicating that the changes in $\bar{R}$ and $\bar{D}$ brought by quenching can be described essentially by thermal contraction. On the other hand, the measured ratios are significantly larger than the calculated ratios when the temperature is raised to 180 °C, indicating that the changes in $\bar{R}$ and $\bar{D}$ must involve a change of N to some extent as well as the thermal expansion.

2. Line Widths of SAXS Peaks. The line width of the first-order SAXS maximum arising from the interparticle interference between nearest-neighbor particles and that arising from the isolated particles are investigated as a function of the heat treatments to investigate, respectively, the distribution of the interdomain distance $\sigma_d/\bar{D}$ and the domain size $\sigma_r/\bar{R}$. Here we assumed that the distribution of the interdomain distance D is Gaussian

$$P(D) = (2\pi\sigma_d^2)^{-1/2} \exp[-(D - \bar{D})^2/2\sigma_d^2] \tag{21}$$

and that the first-order maximum is affected only by the function $P(D)$.

The lattice disordered parameter g ($\equiv\sigma_d/\bar{D}$) was evaluated from diffraction theory of paracrystals, the integral breadth of the first-order peak from the paracrystalline lattice being given by[14,21]

$$\delta\beta = \pi^2 g^2/\bar{D} = \pi^2\sigma_d^2/\bar{D}^3 \quad (22)$$

The integral breadth is associated with the fwhm (W_d) of the observed first-order peak, since the peak can be approximated as Gaussian:

$$\delta\beta = [\pi/(4 \ln 2)]^{1/2} W_d \quad (23)$$

From eq 22 and 23, the g factor can be evaluated since $\bar{D}$ and W_d can be measured experimentally. The results are summarized in Table I. The quantity σ_r/R was estimated as discussed in section III-2.

The g factors are a little larger than the value of $\sigma_r/\bar{R}$. In light of the assumptions involved in estimating the g factors (e.g., the assumptions involved in eq 22), we may regard the g factors as being almost identical with the values $\sigma_r/\bar{R}$ within the errors involved in their assessment. We next consider the temperature dependence of the g factor and $\sigma_r/\bar{R}$.

Suppose the spherical domains are in the field of quasi-elastic force; then the distribution of the interparticle distance D is given by a Gaussian function $P(D)$ in eq 21 with a variance given, from Boltzmann's law, by[15]

$$\sigma_d^2(T) = k_B T/f(T) \quad (24)$$

where $k_B T$ is Boltzmann's free energy and f is a "spring constant", a restoring force for a unit displacement of the interparticle distance; i.e.

$$f(T) = \left(\frac{\partial F}{\partial D}\right)_T = \left.\frac{\partial^2 \Delta G(D,T)}{\partial D^2}\right|_{D=D_{eq},T} \quad (25)$$

where F is a quasi-elastic force acting on the domains and $\Delta G(D,T)$ is the free energy of the domain formation at a given temperature T and interdomain distance D. If the origin of the quasi-elastic force is entropic, then

$$f(T) \propto k_B T \quad (26)$$

Therefore $\sigma_d^2(T)$ is independent of temperature, and therefore the line width should be independent of temperature. On the other hand, if the origin of the force is energetic, then $f(T)$ is less temperature sensitive, consequently leading to increasing σ_d^2 and line width. If $f(T)$ is independent of T, then $\sigma_d(180\,°C)/\sigma_d(\text{room temp}) = 1.23$.

The ratios $\sigma_d(180\,°C)/\sigma_d(\text{room temp})$ and $\sigma_r(180\,°C)/\sigma_r(\text{room temp})$ are 1.41 and 1.64, respectively, when the temperature is raised to 180 °C and are 1.09 and 1.01 when the temperature is lowered from 180 °C to room temperature. The ratios are also calculated from the equilibrium theory of Helfand and Wasserman.[7] If $\psi(T,D)$ is defined as

$$\Delta G(D,T)/(N_{AB} k_B T) \equiv \psi(T,D) \quad (27)$$

where N_{AB} is the number of block polymer chains incorporated cooperatively in the microphase separation, then

$$\frac{\sigma_d(T_1)}{\sigma_d(T_2)} = \frac{[N_{AB}(T_2)\ \partial^2\psi(T_2,D)/\partial D^2]^{1/2}_{D=D_{eq}(T_2)}}{[N_{AB}(T_1)\ \partial^2\psi(T_1,D)/\partial D^2]^{1/2}_{D=D_{eq}(T_1)}} \quad (28)$$

$$\frac{\sigma_r(T_1)}{\sigma_r(T_2)} = \frac{[N_{AB}(T_2)\ \partial^2\psi(T_2,R)/\partial R^2]^{1/2}_{R=R_{eq}(T_2)}}{[N_{AB}(T_1)\ \partial^2\psi(T_1,R)/\partial R^2]^{1/2}_{R=R_{eq}(T_2)}} \quad (29)$$

In order to compare the theoretical ratio σ_d with that experimentally estimated on the basis of eq 22 and 23, the following assumption should be made. The free energy of the domain formation at a given temperature generally depends on the distribution of interdomain distances $\mathbf{D} = \{D_i\}$ and domain radii $\mathbf{R} = \{R_i\}$, where D_i is the i-th interdomain distance and R_i is the radius of i-th sphere. The experimentally estimated σ_d is related to the second-order derivative of the free energy with respect to a given D_r, while all other D's and R's are kept constant; i.e.,

$$\sigma_d^{-2}(T) = \frac{1}{k_B T}\left[\frac{\partial^2 \Delta G(\{D_i\},\{R_i\},T)}{\partial D_r^2}\right]_{\{D_i\}_{eq},\{R_i\}_{eq},T} \quad (i \neq r) \quad (30)$$

On the other hand, the theory assumes all D's are equal to D, and σ_d is obtained from the derivative with all D's varying simultaneously. We assume that these two types of derivatives do not differ by much.

One should note that, in order to calculate absolute value of σ_d, one must know the number of block polymer chains N_{AB} which are cooperatively incorporated in the domain formation. Since this number is unknown experimentally, we discuss here only the relative values of σ_d and σ_r at two different temperatures. Moreover, the equilibrium theory inherently assumes N_{AB} to be a very large number, so even though the quantity $\psi(T,D)$ associated with the free energy of the domain formation per block chain has only a shallow minimum with D or R, the resulting line profiles become extremely sharp like the δ function, i.e., $\sigma_d(T) \to 0$ and $\sigma_r(T) \to 0$. We assume in our treatment that this N_{AB} is relatively small, resulting in the observed line profile. The reduced number N_{AB} may be caused by a nonequilibrium effect involved in the domain formation process which gives rise to isolated grains, each composed of N_{AB} block chains.

Assuming N_{AB} is temperature independent, theory predicts that

$$\frac{\sigma_d(180\ °C)}{\sigma_d(\text{room temp})} = \frac{\sigma_r(180\ °C)}{\sigma_r(\text{room temp})} = 1.02 \quad (31)$$

suggesting that the quasielastic force is entropic in origin. The large values in the observed ratios with temperature elevation, i.e., $\sigma_d(180\,°C)/\sigma_d(\text{room temp}) = 1.41$ and $\sigma_r(180\ °C)/\sigma_r(\text{room temp}) = 1.64$, may be interpreted as arising from disorders set up during the processes for achieving equilibrium at elevated temperature 180 °C. On the other hand, when the samples are quenched from 180 °C to room temperature, the observed ratios are very small, i.e., $\sigma_d(180\,°C)/\sigma_d(\text{room temp}) = 1.09$ and $\sigma_r(180\ °C)/\sigma_r(\text{room temp}) = 1.01$. This occurs because the system does not follow equilibrium within the time scale of the quenching, and nothing happens except for the thermal contraction. Thus the conclusion obtained from the temperature dependence of the profile is in agreement with that obtained from the temperature dependence of $\bar{D}$ and $\bar{R}$.

Table III
Comparisons between Experimental and Predicted Characteristic Interfacial Thicknesses for the Spherical Domain

	domain-boundary thickness ΔR, nm			
		calcd		
condition	exptl	ΔR_{RM}	$\Delta R_{RZ\,1}$	$\Delta R_{RZ\,2}$
room temp	2.1	1.4	1.4	1.8
180 °C	2.5	2.0	2.3	2.5
quenched	1.8	1.4	1.4	1.8
		(1.7)	(1.8)	(2.1)

3. Domain-Boundary Thickness. Table III compares experimental and predicted characteristic interfacial thicknesses for the block polymer. The predicted values are based on the Helfand-Sapse theory:[16]

$$\Delta R = 2[(\beta_A^2 + \beta_B^2)/2\Omega]^{1/2}$$

$$\beta_K^2 = \rho_{0K} b_K^2/6 \quad (32)$$

where b_K and ρ_{0K} are given by eq 16 and 17. The characteristic interfacial thickness ΔR_{RM} was calculated by using the result reported by Rounds and McIntyre on the interaction parameter Ω (eq 20b), while ΔR_{RZ1} and ΔR_{RZ2} were calculated, respectively, by using the results on Ω_1 and Ω_2 reported by Roe and Zin[17]

$$\Omega_1 = -1309 + 8.7 \times 10^5/T \quad (\mathrm{mol/m^3}) \quad (33a)$$

$$\Omega_2 = -443 + 4.2 \times 10^5/T \quad (\mathrm{mol/m^3}) \quad (33b)$$

The results by Roe and Zin, which were obtained on polystyrene and polybutadiene, may not be too much different from those obtained on polystyrene and polyisoprene in light of experimental accuracy in estimating the value of Ω.

Therefore the measured values agree with the predicted values within the experimental errors involved in estimating the value of Ω. The interfacial thickness tends to increase with increasing temperature, which can be accounted for in terms of a decreasing interaction parameter between the constituent block chains with increasing temperature.

Acknowledgment. This work was supported in part by a Grant-in-Aid for Scientific Research from the Ministry of Education, Japan (243021), and by a scientific research grant from the Japan Synthetic Rubber Co., Ltd., Tokyo, Japan, and the Bridgestone Tire Co., Ltd., Tokyo, Japan.

References and Notes

(1) Vanzo, E. V. *J. Polym. Sci., Part A-1* **1966**, *4*, 1727.
(2) Inoue, T.; Soen, T.; Hashimoto, T.; Kawai, H. *J. Polym. Sci., Part A-2* **1969**, *7*, 1283.
(3) Matsuo, M.; Sagae, S.; Asai, H. *Polymer* **1969**, *10*, 79.
(4) Meier, D. J. *J. Polym. Sci., Part C* **1969**, *26*, 81.
(5) Helfand, E. *Macromolecules* **1975**, *8*, 552.
(6) Hashimoto, T.; Fujimura, M.; Kawai, H. *Macromolecules* **1980**, *13*, 1660.
(7) Helfand, E.; Wasserman, Z. R. *Macromolecules* **1978**, *11*, 960.
(8) Hashimoto, T.; Shibayama, M.; Kawai, H. *Macromolecules* **1980**, *13*, 1237.
(9) Hashimoto, T.; Nakamura, N.; Shibayama, M.; Izumi, A.; Kawai, H. *J. Macromol. Sci., Phys.* **1980**, *B17* (3), 389.
(10) Todo, A.; Hashimoto, T.; Kawai, H. *J. Appl. Crystallogr.* **1978**, *11*, 558.
(11) Fujimura, M.; Hashimoto, T.; Kawai, H. *Mem. Fac. Eng. Kyoto Univ.* **1981**, *43* (2), 224.
(12) Hashimoto, T.; Suehiro, S.; Shibayama, M.; Saijo, K.; Kawai, H. *Polym. J.* **1981**, *13*, 501.
(13) Vonk, C. G. *J. Appl. Crystallogr.* **1973**, *6*, 81.
(14) Hosemann, R.; Bagchi, S. N. "Direct Analysis of Diffraction by Matter"; North-Holland Publishing Co.: Amsterdam, 1962.
(15) Prins, J. A. *Naturwissenschaften* **1931**, *19*, 435.
(16) Helfand, E.; Sapse, A. M. *J. Chem. Phys.* **1975**, *62*, 1372.
(17) Roe, R. J.; Zin, W. C. *Macromolecules* **1980**, *13*, 1221.
(18) It should be noted that the samples were heated to 180 °C. However, this temperature is very much below the upper critical solution temperature (UCST) of the block polymer sample, i.e., the temperature at which microphase separation disappears and a homogeneous mixture is obtained. The UCST for this particular block polymer is roughly estimated to be about 350 °C, based on the narrow-interphase approximation of Helfand and Wasserman.[7]
(19) $\bar{v}_K$ is the molecular volume of the K-polymer chain, given by $\bar{v}_K = M_K/(C_K N_A)$, where M_K is the molecular weight of the K polymer, N_A is Avogadro's number, and C_K is the concentration of K polymer in the K-polymer solution (i.e., the weight of K polymer divided by the K-polymer volume plus solvent volume). If d_K is the bulk mass density of K polymer, then $C_K = d_K \phi_K$, where ϕ_K is the volume fraction of K polymer in the K-polymer solution.
(20) The following experiments were conducted to confirm further the above arguments on the temperature dependencies of $\bar{R}$ and $\bar{D}$. The samples heated at 180 °C were slowly cooled to room temperature. The SAXS profiles measured at room temperature showed that the values of $\bar{R}$ and $\bar{D}$ are identical within experimental error to those obtained on the quenched samples. Moreover, the SAXS profiles were also measured at 120 °C on the sample which was heated to 180 °C and subsequently cooled slowly to 120 °C. The results indicated that the values $\bar{R}$ and $\bar{D}$ do not return to those expected for reversible changes in size between those at room temperature and at 180 °C. Rather the values at 120 °C are nearly identical with those for the quenched samples. These results further confirm our conclusions that the increases of $\bar{R}$ and $\bar{D}$ with temperature do not reflect thermal equilibrium but that they occur as a consequence of the system tending to approach equilibrium. The equilibrium and nonequilibrium aspects on the temperature dependencies of the domain size will be discussed in more detail in our forthcoming papers[22] for spherical and lamellar microdomains in bulk and concentrated solutions.
(21) We assume the disorders in the interdomain distance are of ideal-paracrystal type. The validity of the assumption requires further investigation.
(22) Shibayama, M.; Hashimoto, T.; Kawai, H., to be submitted to *Macromolecules*.